Philosophical Magazine

ISSN: 1478-6435 (Print) 1478-6443 (Online) Journal homepage: https://www.tandfonline.com/loi/tphm20

Stable monolayer of the RuO_2 structure by the Peierls distortion

F. Ersan, H. D. Ozaydin & O. Üzengi Aktürk

To cite this article: F. Ersan, H. D. Ozaydin & O. Üzengi Aktürk (2019) Stable monolayer of the RuO_2 structure by the Peierls distortion, Philosophical Magazine, 99:3, 376-385, DOI: 10.1080/14786435.2018.1538576

To link to this article: https://doi.org/10.1080/14786435.2018.1538576

Published online: 29 Oct 2018.

PHILOSOPHICAL MAGAZINE
2019, VOL. 99, NO. 3, 376–385
https://doi.org/10.1080/14786435.2018.1538576

Taylor & Francis
Taylor & Francis Group

Stable monolayer of the RuO_2 structure by the Peierls distortion

F. Ersan [a,b], H. D. Ozaydin[a] and O. Üzengi Aktürk[c,d]

[a]Department of Physics, Adnan Menderes University, Aydın, Turkey; [b]Department of Physics, Faculty of Science, Bilkent University, Ankara, Turkey; [c]Department of Electrical and Electronics Engineering, Adnan Menderes University, Aydın, Turkey; [d]Nanotechnology Application and Research Center, Adnan Menderes University, Aydın, Turkey

ABSTRACT

In this paper, we presented a stable two-dimensional ruthenium dioxide monolayer by using first-principles calculations within density functional theory. In contrast to ordinary hexagonal and octahedral structures of metal dichalcogenides, RuO_2 is stable in the distorted phase of the structure as a result of occurring charge density wave. A comprehensive analysis including the calculation of vibration frequencies, mechanical properties, and *ab initio* molecular dynamics at 300 K affirms that RuO_2 monolayer structure is stable dynamically and thermally and convenient for applications at room temperature. We also investigated the electronic and optical properties of RuO_2 and it is found that RuO_2 has of 0.74 eV band gap which is in the infrared region and very suitable for infrared detectors.

ARTICLE HISTORY
Received 26 January 2018
Accepted 5 October 2018

KEYWORDS
Density functional theory; metal dichalcogenides; two-dimensional materials; charge density wave; Peierls distortion

1. Introduction

After the synthesis of graphene [1], the researcher efforts have been directed towards to explore new two-dimensional (2D) materials not only graphene-like materials but also other ultra-thin crystal structures since which have extra-ordinary physical properties [2, 3] differing from their bulk counterparts. In this regard, similar to graphene; silicene [4, 5], germanene [4–6], stanene [7, 8] and hexagonal III–V binary compounds (h-BN, h- AlN) [9–11] have attracted great interest both the theoretical prediction and also synthesis. Furthermore, the other attractive subject is layered crystals of transition metal dichalcogenides (TMDs) [12–18] owing to their remarkable electronic, mechanical and optical properties. Typical 2D TMDs with a common formula MX_2, which sandwich structure of three atomic layers have been widely explored in recent years due to unique chemical and physical properties that are absent or difficult to

CONTACT F. Ersan fatih.ersan@adu.edu.tr Department of Physics, Adnan Menderes University, 09100 Aydın, Turkey; Department of Physics, Faculty of Science, Bilkent University, 06800 Ankara, Turkey; O. Üzengi Aktürk ouzengi@adu.edu.tr Department of Electrical and Electronics Engineering, Adnan Menderes University, 09100 Aydın, Turkey; Nanotechnology Application and Research Center, Adnan Menderes University, 09100 Aydın, Turkey

obtain in other 2D materials [19–23]. The most well known and studied materials are MX_2 where M = Mo, W, Ti, Ta, Pt, Zr, Re, Ru and X = S, Se [24–29]. For instance, by using a first-principles approach, Li et al. reported the first successful activation and optimisation of a MoS_2 basal plane for hydrogen evolution [30]. Ersan et al. showed new 2D forms of RuS_2 and $RuSe_2$, also they investigated stability, electronic, magnetic, optical, and thermodynamic properties of these structures in detail [31]. In addition to TMDs, transition metal dioxides (TMOs) layers can exist [32, 33], and many studies show TMOs can be good cathode material for alkali (Li, Na) ion batteries [34–37] For the case of TMOs, monolayer manganese dioxide (MnO_2) was synthesised successfully by Omomo et al.[38]. With this motivation, we have studied 2D RuO_2 monolayer systematically based on first-principles density functional theory (DFT) calculations. On the basis of extensive analysis of stability, we determined that 2D forms of T′ -RuO_2 is dynamically stable and it is a direct semiconductor. The paper is organised as follows: Details of the computational methodology are given in Section 2. Structural, electronic and optical properties of monolayer T′ -RuO_2 is presented in Section 3. Finally, we conclude in Section IV.

2. Computational methodology

First-principles plane wave calculations within DFT are carried out using the projector-augmented wave (PAW) potential method [39] as implemented in the Vienna *ab initio* simulation package (VASP) software [40]. The exchange-correlation interaction is treated using the generalised gradient approximation (GGA) in the Perdew–Burke–Ernzerhof form [41]. A plane wave basis set with kinetic energy cut-off of 600 eV is used for all the calculations. The vacuum spacing between the monolayers is chosen 25 Å. By using conjugate gradient method, all atomic positions and lattice vectors in all structures are fully optimised until all the Hellmann–Feynman forces on each atom are less than 0.001 eV/Å and the total energy difference between two successive steps is smaller than 10^{-5} eV. The pressure in the unit cell is kept below ∼0.5 kbar. The van der Waals interaction was assessed by using the DFT-D2 method [42]. The optimisation process is repeated for both spin-polarised and spin-unpolarised states, and determined the minimum ground state energies of the structures. Phonon dispersion curves ((4×4) supercells for H- and T-structure and (4×6) supercell for T′ -RuO_2) are obtained by using the small displacement method (STM) as implemented in PHONOPY code [43] without spin–orbit coupling. The Monkhorst–Pack scheme [44] is used and the grids of k points are (15×15×1) for H and T structure and of (7×15×1) for the T′ -RuO_2 structure was adopted to sample the first Brillouin zone (BZ). To get more accurate results, we also perform band dispersion calculations by the Heyd–Scuseria–Ernzerhof (HSE06) hybrid functional [45, 46]. The screening length of HSE is 0.2/Å, and the mixing rate of the Hartree Fock exchange potential is 0.25.

3. Results and discussion

Atomic configuration of RuO_2 phases together with the labelled atoms which are in their unit cells and lattice parameters versus total energy graph of T′ -RuO_2 are shown in Figure 1. Optimised lattice parameters for T′ -RuO_2 as follows: a=4.76 Å, b = 3.09 Å, and structural parameter are given in Table 1. These values are smaller than previous results which are obtained for T′ -RuX_2 (X=S, Se) structures' lattice constants [31], and compatible with their atomic radii and electronegativities of X atoms. To determine the cohesion between the atoms we calculated the cohesive energy of RuO_2 per triplet. Cohesive energy is obtained from the difference between the total energy of a free X atom in the unit cell and that of the corresponding T′ -RuO_2. According to this calculation 15.97 eV is found for formula unit of T′ -RuO_2. At the end of the geometrical optimisation, we started to check their dynamical stability at T=0 K. As evident in Figure 2, while H- and T-RuO_2 structures have negative phonon frequencies at almost all directions in their BZ, T′ -RuO_2 has positive frequencies over the whole BZ is declared the stability of the structure. Figure 2 also displays the relationships between thermodynamic variables of T′ -RuO_2 structure and the temperature in the range of 0–1000 K. All of these functions are extracted from the calculated phonon dispersion relations at zero pressure by using PHONOPY programme [43]. As can be seen in Figure 2, the thermodynamic variables change dramatically especially at low temperatures below 200 K. While T′ -RuO_2 has almost fixed free energy below 200 K, it goes to negative values with increasing temperature. The entropy of T′ -RuO_2 also increases with temperature as expected. We also present

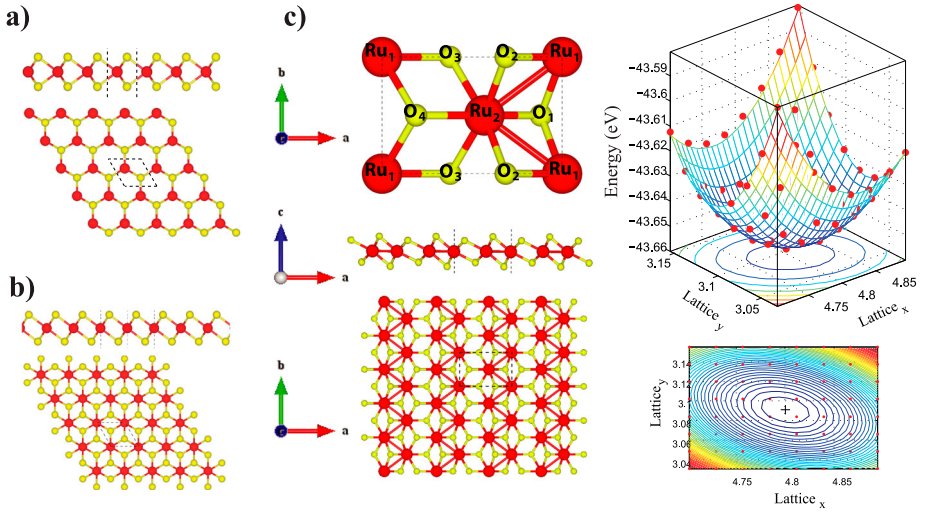

Figure 1. (Color online) a) Side and top view of the H-RuO_2, b) side and top view of the T-RuO_2, c) Unit cell of the T′-RuO_2 structure, side and top view of the expanded T′-RuO_2 is given below and energy versus lattice constant graphs are illustrated at the right panel.

Table 1. The equilibrium optimised structural parameters of T′-RuO_2 monolayer: lattice constants, Ru–Ru and Ru–O distances, band gap energy values for different calculations, charge differences (according to Bader [48] analysis), Poisson's ratio, and in-plane stiffness [50].

Lattice (Å)	Distance (Å)	E_{gap} (eV)	ρ (electrons)	ν_{xy}/ν_{yx}	C_x/C_y (J/m^2)
a=4.76	Ru_1–Ru_2=2.58	PBE=0.12	$Ru_{1,2} = -1.82$	0.253/0.354	118/165
b=3.09	Ru_1–O_1=2.05	PBE+SOC=0.04	$O_{1,4}$=+0.94		
	Ru_1–O_2=1.95	HSE=0.74	$O_{2,3}$=+0.88		
	Ru_2–O_3=2.01				

volumetric specific heat C_v in Figure 2. It is seen that when T<400 K, the heat capacity depends on temperature and according to the third law of thermodynamics, C_v also goes to zero while the temperature goes to zero and at high temperatures, C_v tends to the Dulong–Petit limit. We also check the structural stability of T′ -RuO_2 by molecular dynamic (MD) calculation. MD is performed with Nosé thermostat method at 300 K for 2 ps, and at the end of calculation system remains stable without any deformation. As seen in Figure 1, T′ -RuO_2 is the distorted phase of the T-RuO_2 structure, with this distortion Ru chains in one dimension are occurred in the material, and unstable RuO_2 can be dynamically stable in quasi-2D form. This phase transition can explain by charge density wave (CDW) which is a special case of the Peierls distortion [47]. As is known at low temperature, a wide range of ordered metal atoms in one dimension can undergo a phase transition to achieve lower ground state energy. Some metal atoms can closer to each other and change the periodicity. It results in a double unit cell size. In the present study T′ -RuO_2 structure has ∼0.7 eV lower ground state energy than T-RuO_2 structure. This rearrangement of the Ru atoms creates CDW in T′ -RuO_2 and gains dynamical stability of the structure. Also, electrons at the Fermi level lower their energy with the help of this distortion and the CDWs, so a gap opening at the Fermi level and system turns to semiconductor from metal as seen in Figure 3. Peierls transition means also metal-semiconductor transition [47]. While T-RuO_2 has a metallic character with 1.43 μ_B magnetic moment, T′ -RuO_2 structure shows non-magnetic semiconductor properties with a 0.12 eV direct band gap at Γ point with standard PBE calculation (0.74 eV by HSE calculation). Spin–orbit coupling is

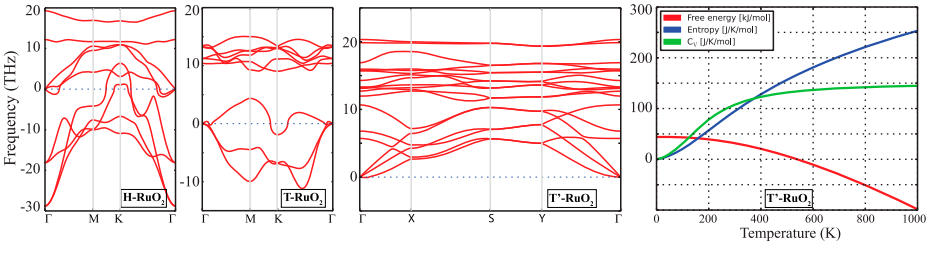

Figure 2. (Colour online) *Ab initio* phonon dispersion curves of H, T, and T′-RuO_2 systems along the main symmetry directions in the 2D Brillouin zone. The thermodynamic results are also presented.

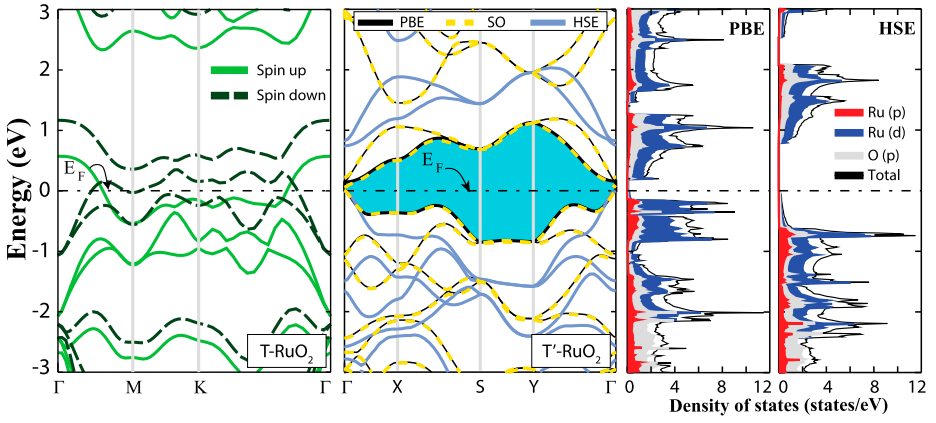

Figure 3. (Colour online) The electronic band structures of T- and T′-RuO_2 monolayers. The orbital projected partial electronic DOS of T′-RuO_2 for the results of PBE and HSE calculations are also presented.

not effective in the whole band structure, SOC is only effective at Γ point and reduces the band gap to 0.04 eV (PBE+SOC). To understand the contribution of the orbitals to the band structure, we plotted the electronic density of states (DOS) for both PBE and HSE calculations. As seen in Figure 3 ruthenium *d* orbitals dominant in the vicinity of Fermi level. Therefore we investigate the effects of CDW on the band structure of T- and T′ -RuO_2 in detail, we plot partial DOS of Ru *d* orbitals as illustrated in Figure 4. Due to the metallic character of T-RuO_2 e_g (d_{z^2}, $d_{x^2-y^2}$) and t_{2g} (d_{xy}, d_{xz}, d_{yz}) orbitals give localised states at the Fermi level. By the CDW unoccupied $d_{x^2-y^2}$ orbital above the Fermi level in the T-RuO_2, becomes fully occupied and shifts to lower energies below the Fermi level in T′ -RuO_2 structure and also d_{z^2} orbital shifts above the Fermi. Similarly, t_{2g} orbitals split from each other and the dominated orbital around valence band maximum is d_{xz}, while d_{xy} and d_{yz} orbitals give the major contribution to the conduction-band minimum. This splitting of orbitals opens a gap

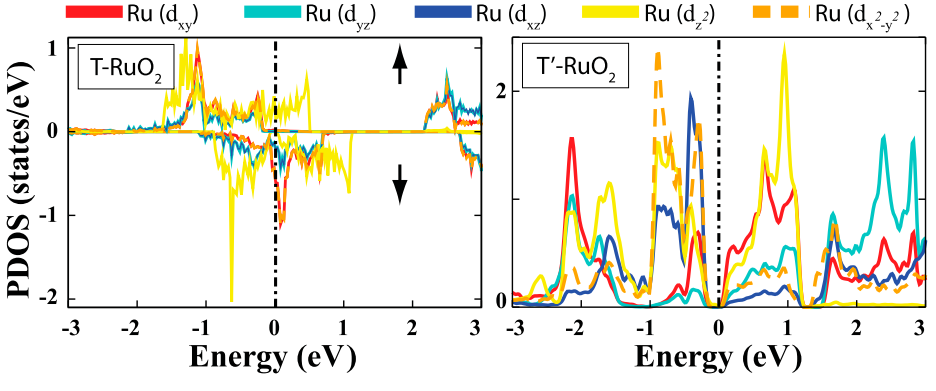

Figure 4. (Colour online) *d* orbital projected partial electronic density of states (PDOS) of T and T′ structures of the RuO_2 monolayer.

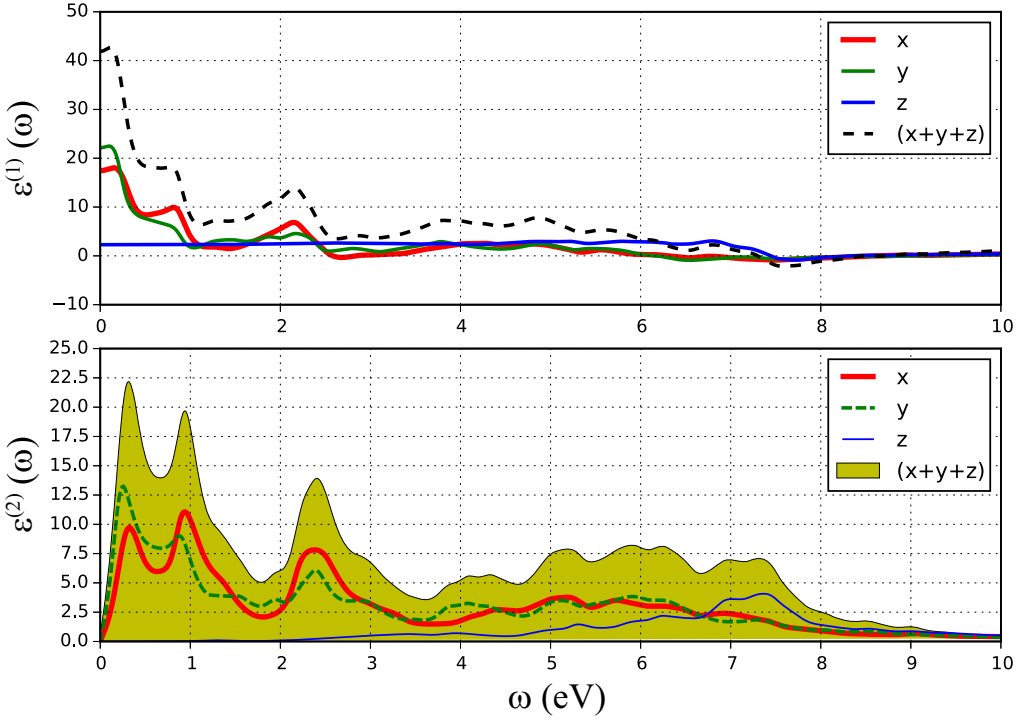

Figure 5. (Colour online) Real $\varepsilon^{(1)}(w)$ and imaginary $\varepsilon^{(2)}(w)$ part of the dielectric response functions as a function of photon energy for T′-RuO_2 monolayer structure.

between the energy levels and makes the T′ -RuO_2 semiconductor materials. According to Bader charge analysis [48], an approximately one electron is transferred from Ru atom to O atom regard as ionic binding between them, while Ru chains have covalent type bonds.

Having a small band gap makes the material be useful in operating devices in the infrared region. Therefore we investigated how the electron in the T′ -RuO_2 gives a response when it absorbs a photon. We calculated the frequency dependent dielectric function $\varepsilon(w)$ of the optimise T′ -RuO_2 monolayer. We note that we exclude the local field effects and also excitonic effects not included in this calculation. The dielectric function has two parts as $\varepsilon(w) = \varepsilon^{(1)}(w) + i\varepsilon^{(2)}(w)$. The imaginary part of $\varepsilon(w)$ is determined by a summation over empty states and the real part of the dielectric tensor $\varepsilon^{(1)}(w)$ is obtained by the usual Kramers–Kronig transformation. These methods are explained in detail by Gajdos et al.[49]. In the present study, the real and imaginary part of the dielectric function is obtained from the PBE calculation. Probably HSE calculation will shift the spectrum nearly 0.6 eV to the higher photon energy. As illustrated in Figure 5, total imaginary part of the dielectric function has three major peaks at 0.32, 0.94 and, 2.42 eV. These first two peaks are in the range of infrared region. We attribute these peaks to the bound-electron transitions from *d* orbital of Ru atoms at the valence band maximum to the *d* orbital of Ru atoms of the conduction band. However T′ -RuO_2 has non-equivalent lattice constants along *x*- and *y*-directions in the unit cell, $\varepsilon^{(2)}(w)_{xx}$ and $\varepsilon^{(2)}(w)_{yy}$ parts of the imaginary dielectric constants approximately have similar trends with increasing photon energy.

4. Conclusions

In conclusion, with our theoretical density functional calculations, we proved RuO_2 can be dynamically stable in the 2D form. The phonon frequency calculations indicate that CDW is occurred by the distortion of Ru atoms and metallic RuO_2 turns to a non-magnetic semiconductor material. We obtained 0.74 eV band gap in the T′ -RuO_2 monolayer by the help of HSE calculations, which is in the near-infrared region. So we believe that T′ -RuO_2 can be suitable for applications in electronic and infrared devices.

Acknowledgments

Computing resources used in this work were provided by the TUBITAK (The Scientific and Technical Research Council of Turkey) ULAKBIM, High Performance and Grid Computing Center (Tr-Grid e Infrastructure).

Disclosure statement

No potential conflict of interest was reported by the authors.

ORCID

Fatih Ersan http://orcid.org/0000-0003-0049-105X

References

[1] K.S. Novoselov, A.K. Geim, S. Morozov, D. Jiang, Y. Zhang, S. Dubunos, I. Grigorieva, and A. Firsov, *Electric field effect in atomically thin carbon films*, Science 306 (2004), pp. 666–669.
[2] M. Chhowalla, H.S. Shin, G. Eda, L.J. Li, K.P. Loh, and H. Zhang, *The chemistry of two-dimensional layered transition metal dichalcogenide nanosheets*, Nat. Chem. 5 (2013), pp. 263–275.
[3] C. Lee, X. Wei, J.W. Kysar, and J. Hone, *Measurement of the elastic properties and intrinsic strength of monolayer graphene*, Science 321 (2008), pp. 385–388.
[4] S. Cahangirov, M. Topsakal, E. Aktürk, H. Sahin, and S. Ciraci, *Two- and one-dimensional honeycomb structures of silicon and germanium*, Phys. Rev. Lett. 102 (2009), pp. 236804.
[5] K. Yang, S. Cahangirov, A. Cantarero, A. Rubio, and R. D'Agosta, *Thermoelectric properties of atomically thin silicene and germanene nanostructures*, Phys. Rev. B 89 (2014), pp. 125403.
[6] M.E. Davila, L. Xian, S. Cahangirov, A. Rubio, and G. Le Lay, *Germanene: A novel two-dimensional germanium allotrope akin to graphene and silicene*, New J. Phys. 16 (2014), pp. 095002.
[7] G.G. Guzman-Verri and C.C. Lew Yan Voon, *Electronic structure of silicon-based nanostructures*, Phys. Rev. B 76 (2007), pp. 075131.
[8] F. -f. Zhu, W. -j. Chen, Y. Xu, C. -l. Gao, D. -d. Guan, C. -h. Liu, D. Qian, S. -C. Zhang, and J. -f. Jia, *Epitaxial growth of two-dimensional stanene*, Nat. Mater. 14 (2015), pp. 1020–1025.
[9] H. Sahin, S. Cahangirov, M. Topsakal, E. Bekaroglu, E. Aktürk, R.T. Senger, and S. Ciraci, *Monolayer honeycomb structures of group-IV elements and III–V binary compounds: First-principles calculations*, Phys. Rev. B 80 (2009), pp. 155453.
[10] P. Tsipas, S. Kassavetis, D. Tsoutsou, E. Xenogiannopoulou, E. Golias, A. Giamini, C. Granzianetti, D. Chiappe, A. Molle, M. Fanciulli, and A. Dimoulas, *Evidence for graphite-like hexagonal AlN nanosheets epitaxially grown on single crystal Ag (111)*, Appl. Phys. Lett. 103 (2013), pp. 251605.
[11] C. Bacaksz, H. Sahin, H.D. Ozaydın, S. Horzum, R.T. Senger, and F.M. Peeters, *Hexagonal AlN: Dimensional-crossover-driven band-gap transition*, Phys. Rev. B 91 (2015), pp. 085430.
[12] R.A. Gordon, D. Yang, E.D. Crozier, D.T. Jiang, and R.F. Frindt, *Structures of exfoliated single layers of WS_2, MoS_2, and $MoSe_2$ in aqueous suspension*, Phys. Rev. B 65 (2002), pp. 125407.
[13] A. Splendiani, L. Sun, Y. Zhang, T. Li, J. Kim, C. -Y. Chim, G. Galli, and F. Wang, *Emerging photoluminescence in monolayer MoS_2*, Nano Lett. 10 (2010), pp. 1271–1275.
[14] J.N. Coleman, M. Lotya, A. O'Neil, S.D. Bergin, P.J. King, U. Khan, K. Young, A. Gaucher, S. De, R.J. Smith, and I.V. Shvets, *Two-dimensional nanosheets produced by liquid exfoliation of layered materials*, Science 331 (2011), pp. 568–571.
[15] C. Ataca, H. Sahin, E. Aktürk, and S. Ciraci, *Mechanical and electronic properties of MoS_2 nanoribbons and their defects*, J. Phys. Chem. C 115 (2011), pp. 3934–3941.
[16] J.S. Ross, P. Klement, A.M. Jones, N.J. Ghimire, J. Yan, D.G. Mandrus, T. Taniguchi, K. Watanabe, K. Kitamura, W. Yao, and D.H. Cobden, *Electrically tunable excitonic light-*

emitting diodes based on monolayer WSe_2 pn junctions, Nat. Nanotech. 9 (2014), pp. 268–272.

[17] H. Sahin, S. Tongay, S. Horzum, W. Fan, J. Zhou, J. Li, J. Wu, and F.M. Peeters, *Anomalous Raman spectra and thickness-dependent electronic properties of WSe_2*, Phys. Rev. B 87 (2013), pp. 165409.

[18] N.R. Wilson, P.V. Nyugen, K. Seyler, P. Rivera, A.J. Marsden, Z.P.L. Laker, G.C. Constantinescu, V. Kandyba, A. Barinov, N.D.M. Hine, and X. Xu, *Determination of band offsets, hybridization, and exciton binding in 2D semiconductor heterostructures*, Sci. Adv. 3 (2017), pp. e1601832.

[19] B. Radisavljevic, A. Radenovic, J. Brivio, V. Giacometti, and A. Kis, *Single-layer MoS_2 transistors*, Nat. Nanotech. 6 (2011), pp. 147–150.

[20] C. Ataca, M. Topsakal, E. Aktürk, and S. Ciraci, *A comparative study of lattice dynamics of three-and two-dimensional MoS_2*, J. Phys. Chem. C 115 (2011), pp. 16354–16361.

[21] H.P. Komsa and A.V. Kranshennikov, *Electronic structures and optical properties of realistic transition metal dichalcogenide heterostructures from first principles*, Phys. Rev. B 88 (2013), pp. 085318.

[22] A. Ramasubramaniam, D. Naveh, and E. Towe, *Tunable band gaps in bilayer transition-metal dichalcogenides*, Phys. Rev. B 84 (2011), pp. 205325.

[23] Y. Li, Z. Zhou, S. Zhang, and Z. Chen, *MoS_2 nanoribbons: High stability and unusual electronic and magnetic properties*, J. Am. Chem. Soc. 130 (2008), pp. 16739–16744.

[24] J. Kang, S. Tongay, J. Zhou, J. Li, and J. Wu, *Band offsets and heterostructures of two-dimensional semiconductors*, Appl. Phys. Lett. 102 (2013), pp. 012111.

[25] S. Tongay, H. Sahin, C. Ko, A. Luce, W. Fan, K. Liu, J. Zhou, Y.S. Huang, C.H. Ho, J. Yan, and D.F. Ogletree, *Monolayer behaviour in bulk ReS_2 due to electronic and vibrational decoupling*, Nat. Commun. 5 (2014), pp. 3252.

[26] H.D. Ozaydin, H. Sahin, J. Kang, F.M. Peeters, and R.T. Senger, *Electronic and magnetic properties of 1T-$TiSe_2$ nanoribbons*, 2D Mater. 2 (2015), pp. 044002.

[27] F. Ersan, Y. Kadioglu, G. Gökoglu, O.Ü. Aktürk, and E. Aktürk, *T-ZrS_2 nanoribbons: Structure and electronic properties*, Philos. Mag. 96 (2016), pp. 2074–2087.

[28] S. Tongay, W. Fan, J. Kang, J. Park, U. Koldemir, J. Suh, D.S. Narang, K. Liu, J. Ji, J. Li, and R. Sinclair, *Tuning interlayer coupling in large-area heterostructures with CVD-grown MoS_2 and WS_2 monolayers*, Nano Lett. 14 (2014), pp. 3185–3190.

[29] W. Zhang, Z. Huang, W. Zhang, and Y. Li, *Two-dimensional semiconductors with possible high room temperature mobility*, Nano Res. 7 (2014), pp. 1731–1737.

[30] L. Hong, T. Charlie, A. Leen, C. Lili, and W.C. Alex, *Activating and optimizing MoS_2 basal planes for hydrogen evolution through the formation of strained sulphur vacancies*, Nat. Mater. 15 (2016), pp. 48–53.

[31] F. Ersan, S. Cahangirov, G. Gökoglu, A. Rubio, and E. Aktürk, *Stable monolayer honeycomb-like structures of RuX_2 (X=S, Se)*, Phys. Rev. B 94 (2016), pp. 155415.

[32] C. Ataca, H. Sahin, and S. Ciraci, *Stable, single-layer MX_2 transition-metal oxides and dichalcogenides in a honeycomb-like structure*, J. Phys. Chem. C 116 (2012), pp. 8983–8999.

[33] F.A. Rasmussen and K.S.J. Thygesen, *Computational 2D materials database: Electronic structure of transition-metal dichalcogenides and oxides*, Phys. Chem. C 119 (2015), pp. 13169–13183.

[34] S. Deng, L. Wang, T. Hou, and Y.J. Li, *Two-dimensional MnO_2 as a better cathode material for lithium ion batteries*, Phys. Chem. C 119 (2015), pp. 28783–28788.

[35] Y. Zhou and C. Geng, *A MoO_2 sheet as a promising electrode material: Ultrafast Li-diffusion and astonishing Li-storage capacity*, Nanotechnology 28 (2017), pp. 105402.

[36] G. Li, X. Yue, G. Luo, and J. Zhao, *Electrode potential and activation energy of sodium transition-metal oxides as cathode materials for sodium batteries: A first-principles investigation*, Comput. Mater. Sci. 106 (2015), pp. 15–22.
[37] F. Ersan, H.D. Ozaydın, G. Gökoglu, and E. Aktürk, *Theoretical investigation of lithium adsorption, diffusion and coverage on MX_2 (M= Mo, W; X= O, S, Se, Te) monolayers*, Appl. Surf. Sci. 425 (2017), pp. 301–306.
[38] Y. Omomo, T. Sasaki, L.Z. Wang, and M. Watanabe, *Redoxable nanosheet crystallites of MnO2 derived via delamination of a layered manganese oxide*, J. Am. Chem. Soc. 125 (2003), pp. 3568–3575.
[39] P.E. Blöchl, *Projector augmented-wave method*, Phys. Rev. B 50 (1994), pp. 17953.
[40] G. Kresse and J. Furthmuller, *Efficient iterative schemes for ab initio total-energy calculations using a plane-wave basis set*, Phys. Rev. B 54 (1996), pp. 11169.
[41] J.P. Perdew, K. Burke, and M. Ernzerhof, *Generalized gradient approximation made simple*, Phys. Rev. Lett. 77 (1996), pp. 3865.
[42] S. Grimme, *Semiempirical GGA-type density functional constructed with a long-range dispersion correction*, J. Comput. Chem. 27 (2006), pp. 1787–1799.
[43] A. Togo and I. Tanaka, *First principles phonon calculations in materials science*, Scr. Mater. 108 (2015), pp. 1.
[44] H.J. Monkhorst and J.D. Pack, *Special points for Brillouin-zone integrations*, Phys. Rev. B 13 (1976), pp. 5188.
[45] J. Heyd, G.E. Scuseria, and M.J. Ernzerhof, *Hybrid functionals based on a screened Coulomb potential*, Chem. Phys. 118 (2003), pp. 8207–8215.
[46] A.V. Krukau, O.A. Vydrov, A.F. Izmaylov, and G.E.J. Scuseria, *Influence of the exchange screening parameter on the performance of screened hybrid functionals*, Chem. Phys. 125 (2006), pp. 224106.
[47] I.B.J. Bersuker, *The Jahn–Teller and pseudo Jahn–Teller effect in materials science*, Phys.: Conf. Ser. 833 (2017), pp. 012001.
[48] G. Henkelman, A. Arnaldsson, and H. Jonsson, *A fast and robust algorithm for Bader decomposition of charge density*, Comput. Mater. Sci. 36 (2006), pp. 354–360.
[49] M. Gajdos, K. Hummer, G. Kresse, J. Furthmller, and F. Bechstedt, *Linear optical properties in the projector-augmented wave methodology*, Phys. Rev. B 73 (2006), pp. 045112.
[50] M. Topsakal, S. Cahangirov, and S. Ciraci, *The response of mechanical and electronic properties of graphane to the elastic strain*, Appl. Phys. Lett. 96 (2010), pp. 091912.